Materials Science & Engineering C 113 (2020) 110966

Contents lists available at ScienceDirect

Materials Science & Engineering C

journal homepage: www.elsevier.com/locate/msec

Plasma polymerised nanoscale coatings of controlled thickness for efficient solid-phase presentation of growth factors

Andres Alba-Perez[1], Vineetha Jayawarna[1], Peter G. Childs, Matthew J. Dalby, Manuel Salmeron-Sanchez*

Centre for the Cellular Microenvironment, University of Glasgow, Glasgow, UK

ARTICLE INFO

Keywords:
Plasma polymerisation
Poly(ethyl acrylate)
Growth factors
Stem cells
BMP-2
Fibronectin

ABSTRACT

The engineering of biomaterial surfaces and scaffolds for specific biomedical and clinical application is of growing interest. Certain functionalised surfaces can capture and deliver bioactive molecules, such as growth factors (GF), enhancing the clinical efficacy of such systems. With a custom-made plasma polymerisation reactor described here we have developed bioactive polymer coatings based on poly(ethyl acrylate) (PEA). This remarkable polymer unfolds fibronectin (FN) upon adsorption to allow the GF binding region of FN to sequester and present GFs with high efficiency. We systematically evaluate process conditions and their impact on plasma polymerised PEA coatings and characterise the effect of plasma power and deposition time on thickness, wettability and chemical composition of the coatings. We demonstrate that functional substrate roughness can be maintained after deposition of the polymer coatings. Importantly, we show that coatings deposited at different conditions all maintain a similar or better bioactivity than spin coated PEA references. We show that in PEA plasma polymerised coatings FN assembles into nanonetworks with high availability of integrin and GF binding regions that sequester bone morphogenetic protein-2 (BMP-2). We also report similar mesenchymal stem cell adhesion behaviour, as characterised by focal adhesions, and differentiation potential on BMP-2 coated surfaces, regardless of plasma deposition conditions. This is a potent and versatile technology that can help facilitate the use of GFs in clinical applications.

1. Introduction

Surface modification is a versatile and potent tool in the development of new biomaterials for tissue engineering. Surface treatment technologies can critically improve cell-material interactions and specific functional properties of the material in a biological environment. Modifications related to mechanical properties (e.g. elasticity) [1,2], topographical features (e.g. wettability) [3,4] and chemical composition [5,6] can be found in many biomaterial developments. With a proper modification strategy, a material's surface can be tailored to improve cellular biocompatibility, improving cell adhesion [7], proliferation [8] and differentiation [9], amongst other functional changes.

Intense research effort has been directed towards surface modifications, including chemical treatments for etching [10], UV [11], ozone treatment [12], radiation exposure [13] and the addition of micro and nanoscale surface coatings [14]. Plasma polymerisation has received increased attention in biomaterials engineering due to its ability to deposit a highly crosslinked, nanometric, thin film of polymer at the cell-material interface [15]. Plasma polymerisation (specifically plasma enhanced chemical vapour deposition, PECVD) relies on the generation of an ionised gas where electrons are excited to high energy states using applied electric fields, resulting in glow discharge [16]. Chemically reactive species (e.g. ions, radicals) are then able to interact with the substrate material and undergo polymerisation at this interface creating a film that adheres firmly to the substrate. The process can be carried out with a variety of electrode configurations that typically involve low pressure and low temperatures.

Plasma polymerisation is regarded as an inexpensive and versatile tool to coat biomaterials allowing modified surface chemistry for improved cell adhesion and growth. Unlike conventional wet-chemical polymerisation, where defined polymer chains from monomers form the backbone of the polymer [17], plasma polymerisation involves recombination of monomeric units by cross-linking following fragmentation to produce a randomly structured polymer. This solvent-free process deposits an even thin film that can withstand chemical and physical treatments on complex biodegradable structures. The specific

* Corresponding author.
E-mail address: manuel.salmeron-sanchez@glasgow.ac.uk (M. Salmeron-Sanchez).
[1] These authors contributed equally to this work.

https://doi.org/10.1016/j.msec.2020.110966
Received 1 January 2020; Received in revised form 1 April 2020; Accepted 11 April 2020
Available online 13 April 2020

benefits of plasma polymerisation include a) time-efficient deposition; b) pinhole-free, highly cross-linked structure for a high level of substrate to coating adhesion; c) solvent-free techniques, minimising potential cytotoxicity; d) efficient deposition in 3D porous structures based on plasma diffusion; e) deposition without pre-treatment; f) chemically stable and physically durable coatings; g) fine control of thickness, down to tens of nanometres, for biodegradable applications, and h) non-hostile character to avoid structural alterations of the substrate biomaterial [15,18,19].

Plasma polymerisation by radio frequency (RF) glow discharge can be used to deposit polymer films onto a variety of substrates such as metals, ceramics and other polymers [20]. Academic institutions across the world use a variety of plasma chambers in their labs; while some are custom-made others are commercial devices available from specialised manufacturers. Bespoke equipment is often used following design constraints and prototypes set out several decades ago [21,22], allowing flexibility and cost advantages. However, this presents intrinsic variation in performance, even when based on the same design. Deposition rate, plasma pressure, film uniformity, amongst others are generally specific to each individual system, and calibration and quality testing is needed for new plasma chambers.

Plasma treatments using non-polymerizing gases for the incorporation of various chemical functionalities such as amino [23,24], hydroxyl [25] and carboxyl [26,27] groups have also been used in the past for enhancing the covalent coupling of proteins and biomolecules to substrate biomaterials. Our lab has previously shown the outstanding functional properties of poly(ethyl acrylate) (PEA), unfolding the conformation of fibronectin (FN) upon adsorption and in turn supporting highly efficient presentation of growth factors (GF) in-vitro and in-vivo [28,29]. PEA is a polymer that induces nanofibrillar FN organisation, leading to the exposure of its integrin and GF binding domains. In our previous studies we have shown that plasma-polymerised PEA coatings are similarly able to promote FN assembly and effective presentation of ultra-low doses of bone morphogenetic protein-2 (BMP-2) GF. This drives a synergistic signalling with enhanced human mesenchymal stem cell (hMSC) osteogenesis in vitro and bone formation in vivo, demonstrating the potential of this technology for clinical application in bone regeneration. In this paper we describe in detail the practical and design considerations of our custom-made plasma equipment used to produce PEA nanocoatings. We characterise the physico-chemical properties of the plasma polymerised surfaces and evaluate their effects on hMSC adhesion and differentiation in vitro.

2. Materials and methods

2.1. Plasma equipment set-up

A custom-built plasma reactor was used to polymerise ethyl acrylate (EA) (Sigma, St. Louis, MO) onto microscopy glass coverslips via plasma polymerisation. To develop our system, we have followed previous working designs of bespoke plasma chambers used to polymerise other monomers [30]. Our system is a low-pressure T-shaped plasma reactor vessel made of borosilicate (De Dietrich) and aluminium end plates (custom made in lab workshop) sealed with Viton O-rings with a total volume of around 15 L. Vacuum was produced via rotary or scroll pump (both BOC Edwards), with operating pressures from 5.0×10^{-3} to 6.0×10^{-1} mbar. The plasma was initiated via two capacitively coupled copper band electrodes situated externally to the reactor chamber and connected to a radio frequency power supply (Coaxial Power System Ltd.) that works at 13.56 MHz up to 300 W. The monomer pressure was controlled via speedivalves (BOC Edwards) and monitored with a pirani gauge (Kurt J. Lesker). Details of other design and operation considerations to facilitate the polymerisation of EA can be found in the Supplementary Material section.

In the Supplementary Material section, we have detailed operating protocols to choose our optimal working pressures for each plasma power and to adjust them in a systematic manner for every experiment (Supp. Fig. 1 and Table 1).

2.2. Materials

2.2.1. Plasma PEA surface preparation

Circular 12 mm diameter microscopy glass coverslips (borosilicate glass D263™ M, Marienfeld GmbH & Co.KG, Germany) were used as substrates for the polymer coating. Glass coverslips were cleaned by sonication in ethanol for 30 mins and dried in a lab oven prior to use. As a first stage of every plasma experiment, samples were exposed to air plasma for 5 min at 100 W of RF incident power to ensure removal of any residual organic matter. The plasma polymerisation conditions used in this work were controlled by two parameters: RF power applied to the plasma chamber and plasma treatment time. We used six plasma conditions for this work: 100 W 30 mins (180 kJ), 50 W 30 mins (90 kJ), 50 W 15 mins (45 kJ), 25 W 15 mins (22.5 kJ), 50 W 5 mins (15 kJ), 15 W 5 mins (4.5 kJ).

2.2.2. Spin-coated PEA surface preparation

Spin coated PEA samples were prepared on the same 12 mm glass coverslips from a 4% solution in toluene (Sigma, St. Louis, MO) of bulk PEA, obtained via polymerisation of EA using 1% benzoin (Sigma, St. Louis, MO) as a photoinitiator. Spin coating was operated at a speed of 3000 rpm with an acceleration of 3000 rpm s^{-1} for 30s and vacuum dried at 60 °C for 2 h to extract excess toluene.

2.2.3. PLA surface preparation

Amorphous and crystalline polylactic acid (PLA) (Purasorb PL 18, Corbion, Amsterdam) surfaces were prepared for roughness conservation experiments. Spin coated PLA samples were prepared on 12 mm glass coverslips from 2% solution in chloroform (Sigma, St. Louis, MO) of bulk PLA (amorphous PLA). To obtain crystalline PLA surfaces, spin coated samples underwent thermal treatments. To yield a crystalline PLA surface with small spherulites, samples were put in an oven at 200 °C for 5 min, then at 75 °C for 6 h, and finally at 110 °C for 2 h (crystalline high roughness PLA). To yield a crystalline PLA surface with big spherulites, samples were put in an oven at 200 °C for 5 min, and then at 110 °C for 2 h (crystalline low roughness PLA).

For cell culture experiments samples were sterilised by UV exposure for 30 mins immediately prior to use.

2.3. Atomic force microscopy (AFM)

AFM was used in air for imaging and characterising surface topography of all coated surfaces before and after fibronectin (FN) adsorption. For FN (R&D Systems) coated samples: After coating, samples were washed with water and dried with gentle nitrogen flow before imaging. A JPK Nanowizard 4 (JPK Instruments) system was used in tapping mode for imaging using antimony-doped Si cantilevers with a nominal resonant frequency of 75 kHz (MPP-21220, Bruker). The phase signal was set to 0 at a frequency 5–10% lower than the resonant frequency. Height and phase images were acquired from each scan. The JPK Data Processing software versions 5 and 6 were used for image analysis.

For an estimation of the coating thickness, a thin scratch was manually applied with a sharp blade into the coating, to expose the underlying glass substrate. The surface was then viewed under a microscope to identify the scratch, and the area across the cut scanned by AFM. The thickness of the polymer coating was estimated by profilometry at the boundary of the scratched and unscratched area, n = 5 (minimum).

2.4. Water contact angle (WCA)

Water contact angle measurements were taken on all coated

surfaces before and after FN coating. Static contact angles (SCAs) were measured by dropping 3 μL drop of deionised water on to the surfaces using a Theta optical tensiometer (Biolin Scientific, Stockholm, Sweden). The stability of the coatings was also checked up to 14 days after undertaking the plasma/spin coating treatment.

2.5. X-ray photoelectron spectroscopy (XPS)

X-ray photoelectron spectroscopy was used to identify the surface chemical composition of coated samples. All X-ray photoelectron spectra were obtained at the National EPSRC Users' Service (NEXUS) at Newcastle University (found at: http://www.ncl.ac.uk/nexus/). Each sample was analysed at three points with a maximum beam size (400 μm × 800 μm) with a K-alpha XPS system (Thermo Scientific) equipped with a monochromatic Al K-alpha source for carbon, oxygen and overview spectra. X-ray energy was 1486.68 eV at a voltage of 12 kV, current of 3 mA and power of 36 W. Spectra analysis and curve fitting were performed using CasaXPS software version 2.3.16.

2.6. Micro Bicinchoninic acid protein quantification assay (BCA)

The density of adsorbed protein was determined by measuring the amount of non-adsorbed FN. A standard curve was created via serial dilutions of a FN stock of known concentration. Samples were coated for 1 h and the remaining FN solution was transferred to 96-well plates, where the bicinchoninic acid working reagent was added (Thermo Fisher Scientific, Waltham, MA). The plate was then agitated and incubated at 37 °C for 2 h. The absorbance was read at 562 nm with a Tecan NanoQuant Infinite M200 Pro plate reader (Männedorf, Switzerland).

2.7. Immunostaining of fibronectin

Immunostaining was done with polyclonal anti-FN (Sigma) primary antibody directed against FN. PEA surfaces were coated using a 20 μg/mL FN solution in DPBS for 1 h. Surfaces were then washed in DPBS and fixed with 4% formaldehyde at 4 °C for 30 min. The samples were then blocked with 1% BSA/DPBS for 30 min at room temperature and incubated with anti-FN (1:200 dilution in DPBS/BSA 1% w/v) for 1 h at room temperature. After three washes with DPBS/0.5% Tween 20, samples were incubated with Cy3 anti-mouse secondary antibody (1:200 in DPBS/BSA 1% w/v) for 1 h at room temperature. Finally, the samples were rinsed in DPBS/0.5% Tween 20 and mounted with vectashield (Vector Laboratories) and imaged using an epifluorescence microscope (ZEISS Axio Observer Z1).

2.8. Protein adsorption assays

ELISA was performed to assess the exposure of specific domains on the FN molecule. Surfaces were coated using a 20 μg/mL FN solution in DPBS for 1 h, followed by blocking for 30 min with 1% bovine serum albumin (Sigma-Aldrich) in DPBS. Subsequently, primary antibodies for the FN($III_{9–10}$) domain (HFN7.1, mouse monoclonal, 1:330, Developmental Studies Hybridoma) and FN($III_{12–14}$) domain (P5F3, mouse monoclonal, 1:2000, Santa Cruz Biotechnology) were added onto the surfaces and incubated for 1 h. The surfaces were thereafter washed 3 × 5 min with 0.5% Tween 20 in DPBS. A horseradish peroxidase (HRP)-conjugated anti-mouse antibody (1:10000, Thermo Fisher) was then added onto the surface and incubated for 1 h in the dark, followed by washing for 3 × 5 min with 0.5% Tween 20 in DPBS. Afterwards, a substrate solution (R&D Systems) was added onto the surfaces and the samples were incubated in the dark for 20 min, followed by the addition of a stop solution (R&D Systems). The absorbance of the coloured solution was read at 450 and 540 nm and the data were used to determine the relative exposure of the FN domains. All procedures were performed at room temperature.

2.9. Quantification of BMP-2 adsorption

The density of adsorbed BMP-2 was determined by measuring the amount of non-adsorbed BMP-2 that remained in the supernatant via sandwich ELISA (R&D System) following the manufacturer's instructions. Briefly, in this process, ELISA plates were coated with the capture antibody before they were blocked with bovine serum albumin for 1 h. After appropriately diluted supernatants were added, bound BMP-2 was detected with biotinylated anti-human BMP-2 antibody. Streptavidin conjugated horseradish peroxidase was then added to the plates. Enzyme substrate was treated for 20 min before the reaction was stopped by adding an acidic solution. Absorbance was measured at 450 nm with wavelength correction at 570 nm. The standard curve was calculated using a four parameter logistic (4-PL) curve fit. The amount of adsorbed BMP-2 was calculated from a standard curve based on known concentrations of BMP-2.

2.10. Cell culture

Primary bone marrow MSCs from Promocell were used for the experiments. The basal medium that was used to maintain MSCs was DMEM (Sigma-Aldrich) supplemented with 10% FBS (Sigma), 1% sodium pyruvate (sigma), 1% non-essential amino acids (Thermos Fisher Scientific) and 2% antibiotics (6.74 U mL^{-1} penicillin-streptomycin, 0.2 μg/ mL fungizone and 2 mM L-glutamine). Cells (5000 cells per sample) were seeded onto the materials along with medium (DMEM, 1% sodium pyruvate, 1% non-essential amino acids, 2% antibiotics and 5% FBS) which was changed twice a week. All cell cultures were performed in an incubator at 37 °C with 5% CO_2. Expanded MSCs were used at passages 1–3.

2.11. Immunofluorescence staining for cell adhesion (vinculin)

After each culture time, cells were washed in DPBS and fixed with 4% formaldehyde at 37 °C for 15 min. Afterwards, the samples were rinsed in DPBS and a permeabilizing buffer [10.3 g of sucrose, 0.292 g of NaCl, 0.06 g of $MgCl_2$, 0.476 g of Hepes buffer, 0.5 mL of Triton X, in 100 mL of PBS (pH 7.2)] was added at 4 °C for 5 min. The samples were then blocked with 1% BSA/DPBS at 37 °C for 15 min. Subsequently, they were incubated at 37 °C for 1 h with a primary antibody against vinculin (monoclonal mouse antibody, Sigma, 1:150) and with phalloidin (Invitrogen, 1:200) to stain actin in 1% BSA/DPBS. After three washes with PBS/0.5% Tween 20, the appropriate biotinylated anti-mouse secondary antibody (Vector Laboratories, 1:50) was incubated for 1 h at 37 °C, followed by fluorescein streptavidin tertiary label (Vector Laboratories, 1: 50) for 30 min at 4 °C. Finally, the samples were rinsed in PBS/0.5% Tween 20 three times before mounting in Vectashield containing DAPI stain (Vector Laboratories). An Axiovert 200 M fluorescence microscope was used for imaging.

2.12. Quantitative real-time PCR

After each culture time, total RNA was extracted using Qiagen RNeasy micro kit (including a DNAse step) according to the manufacturer's instructions. The RNA concentration was quantified using nanodrop and normalized for each sample. cDNA was prepared by reverse transcription using the Qiagen Quantitect kit (Applied Biosystems) also according to the manufacturers' protocol. The Quantifast SYBR green qRT-PCR kit (Qiagen) was used to perform amplification with specific primers (Eurofins Genomics, Ebersberg, Germany) related to osteogenesis, listed in Supplementary (Supp. Table 2). Gene expression levels were standardized using GAPDH as a genetic internal control. qRT-PCR products were quantified using the ΔΔCt method and amplification was carried out using an Applied Biosystems 7500 Real Time PCR system.

2.13. Von Kossa staining

After 28 days, culture samples were fixed with 4% formaldehyde for 15 min at 37 °C. Samples were then submerged in 5% silver nitrate solutions and exposed to UV light for 30 min. After washing in deionised water, 5% sodium thiosulphate was added to the sample for 10 min and then samples were washed with warm tap water for 10 mins. After another wash with deionised water, the samples were counter-stained with nuclear fast red for 10 min and washed again with deionised water. Finally, the samples were rinsed with 70% ethanol and observed in a phase-contrast optical microscope (Zeiss Axio Observer Z1).

2.14. Statistical analysis

All statistical analysis was performed with GraphPad Prism 6. Data is presented as mean ± SD and analysed with ANOVA with a Tukey post-hoc test. Statistical significance levels are *p < 0.05, **p < 0.01 and ***p < 0.001.

3. Results and discussion

3.1. Plasma polymerisation of ethyl acrylate by radio frequency glow discharge

We have chosen a low pressure, low power plasma polymerisation reactor design that allows control of the thickness and chemical integrity of the functional coating. A schematic of the system is presented in Fig. 1. To develop our system, we have followed previous working designs of lab plasma chambers used to polymerise other monomers [31], adapting specific design and operation requirements to the particular constraints of working with ethyl acrylate (EA) monomer.

For the experiments in this study we first established a plasma deposition protocol that allowed control of the flow of monomer and level of vacuum needed to spark and stabilize a plasma reaction. Our detailed operation protocol and design considerations are included in the Supplementary Materials section.

3.2. Characterisation of plasma polymerised surfaces

Glass coverslips were coated with plasma polymerised ethyl acrylate (pPEA) at different RF powers and durations. Experiments were performed after thorough cleaning of the reactor inner walls, to minimize ablation residues being deposited on the sample surfaces. Samples were produced at powers ranging from 15 W to 100 W for durations of 5 to 30 min -which gives a broad range of energies used in the polymerisation process (from 4.5 to 180.0 kJ). Experimental conditions are shown in Table 1. We used radically polymerised spin-coated PEA (SC-PEA) as a positive reference surface to compare functional features, as this material has demonstrated FN network formation in previous studies [28].

Table 1
Sample coating conditions tested and measured thickness of coatings with an AFM scratch test.

Sample condition		Energy (kJ)	Thickness (nm)	Coating rate (nm/min)
Plasma power (W)	Time (min)			
15	5	4.5	34 ± 7	6.8 ± 1.4
50	5	15.0	43 ± 7	8.6 ± 1.4
25	15	22.5	118 ± 14	7.9 ± 0.9
50	15	45.0	138 ± 22	9.2 ± 1.5
50	30	90.0	236 ± 10	7.9 ± 0.3
100	30	180.0	309 ± 28	10.3 ± 0.9
Spin coating		–	1272 ± 117	–

Surface properties of all coated samples were characterised by AFM, water contact angle (WCA) and X-ray photoelectron spectroscopy (XPS). AFM scans were used to characterise surface topography and thickness of the coatings. After plasma deposition, all surfaces with pPEA showed similar features: a homogeneously flat surface covered with polymerised material and randomly distributed flakes or specs of slightly softer polymerised material (Supp. Fig. 2).

The deposition rate of the plasma polymerised materials on the sample surfaces has been characterised by measuring the thickness of coatings deposited at various experimental conditions. We used AFM to measure the depth of a clean scratch performed on the surface of a sample after polymer deposition (Fig. 2A). The scratch was made carefully by running a razor along the surface of a coated sample as to scratch the polymerised material on the surface down to the underlying glass. By changing the parameters of the plasma deposition experiments, these scratch tests have shown that the deposition rate remains fairly constant during the monomer plasma polymerisation stage for a given process pressure. With our system we achieved rates from around 6.5 nm/min to over 10 nm/min and we were able to produce nano scale coatings onto glass ranging from 34 ± 7 to 309 ± 28 nm for

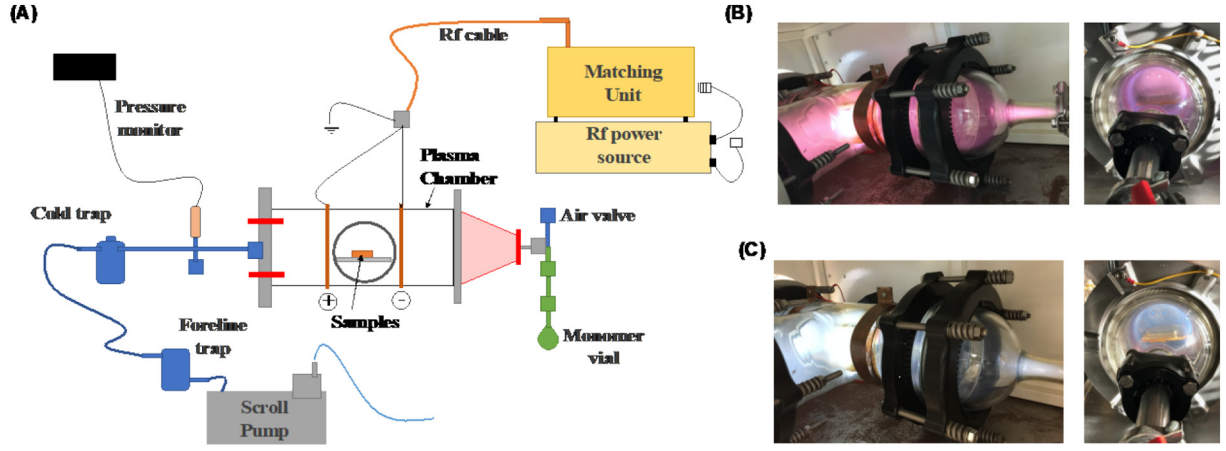

Fig. 1. Custom made plasma reactor. (A) Schematic representation of plasma polymerisation apparatus. A scroll pump is used to lower air pressure inside a plasma chamber, a cylindrical glass chamber with inlets for air and monomer from a connected glass vial, and with a side lid for access to the sample holder. The pump is protected from chemicals by a cold trap, filled with liquid N2 during experiments. Electrodes are copper rings wrapped radially outside the chamber connected to a radiofrequency (RF) power source though an RF cable. (B) Sparked with an air plasma (side and front view of chamber) and (C) a monomer plasma (side and front view of chamber).

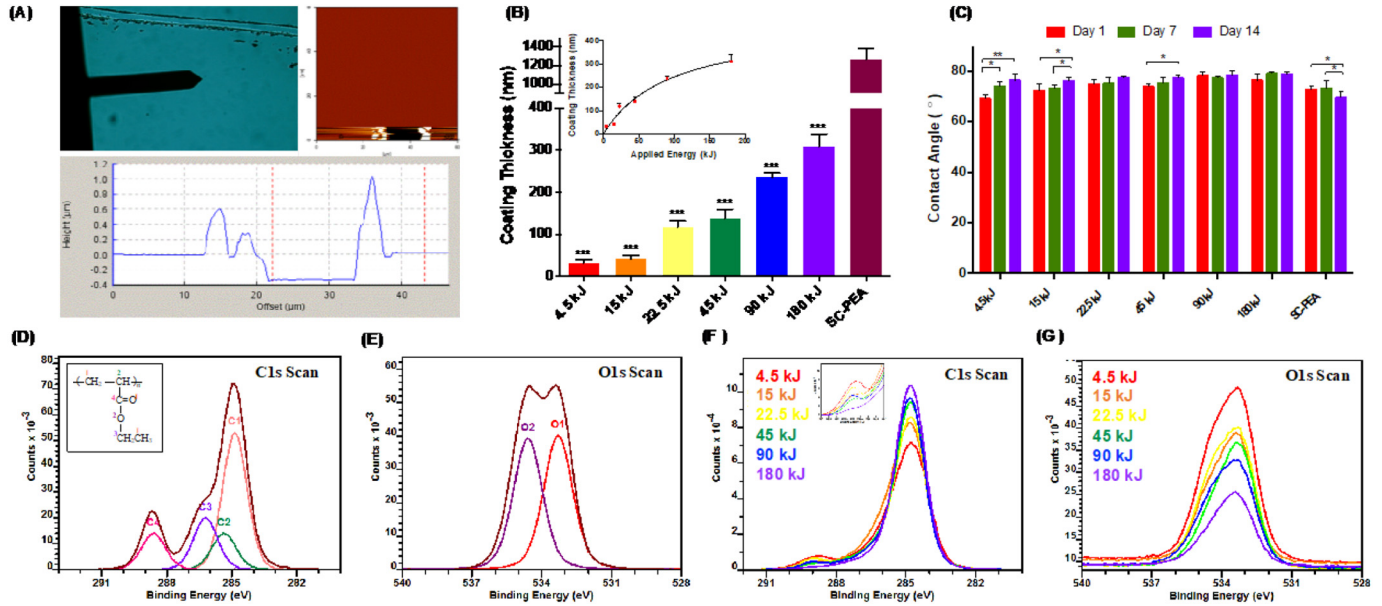

Fig. 2. Characterisation of PEA coatings on glass coverslips deposited at various conditions. (A) Example of a scratch test on a coated pPEA surface at 180 kJ. Upper - seen under an optical microscope (scratch with AFM tip) and AFM scan image. Lower - a scratch profile as measured with AFM. (B) Thickness of the PEA coatings is measured with AFM of a scratch in the polymer. Thickness of the coatings increased with increasing energy. SC-PEA showed significantly higher thickness compared to plasma coatings. (C) Water contact angle of PEA coatings deposited at various conditions, measured up to 14 days after leaving samples in air, n = 3 (minimum). Values remain unchanged at different time points after deposition. D-G) Chemical composition of the PEA surface measured by XPS analysis. D, E) C1s and O1s core-level spectra of SC-PEA with fitted peaks which represent binding conformations of carbon and oxygen atoms on the top 10 nm of the sample surfaces. The inset shows chemical structure of PEA, with labelled carbon and oxygen atoms corresponding to components as indicated on C1s and O1s scans. F, G) Overlaid C1s and O1s core-level spectra of pPEA samples produced at varying powers, showing generally that increasing power results in decreasing ester and carboxyl side chains on the produced PEA.

depositions at 4.5 kJ and 180 kJ respectively (Table 1, Fig. 2B). Thickness of the coatings thickness increased with increasing power. The relationship between the applied energy and the obtained PEA coating seems to follow a hyperbolic curve model (Fig. 2B inset). As a reference, SC-PEA produced coatings of thickness well over one micron. The consistency of deposition rate at different points within the chamber was assessed in a similar manner by placing coverslips on twenty-two different positions throughout the chamber including ten onto the sample holding shelf in the middle of the chamber. We found moderate variations on deposition rate (Supp. Fig. 3) along the chamber, with average values from around 5 to 10 nm per minute with depositions at a 90 kJ plasma, with the exception of the area under the back (inlet) electrode that produced much faster deposition rates.

The stability of the plasma coatings was evaluated up to 14 days of storage under dry conditions. We measured static water contact angles (SCA) at different time points (Fig. 2C) and verified that wettability of the surfaces measured by SCA remains fairly unchanged during this time frame. This means that surfaces coated with our system retain functionality and future applications of this technology can use materials that have been stored before in vivo or in vitro use, without losing functionality.

X-ray photoelectron spectroscopy (XPS) measurements were performed to study the chemical composition on the PEA deposited surfaces. SC-PEA was analysed via peak fitting of the carbon (C1s) and oxygen (O1s) spectra (Fig. 2D and E), showing peak positioning and binding ratios similar to those found in literature [32]. C1s spectra were peak fitted with respect to the primary hydrocarbon backbone signal at 285 eV the other three carbon moieties respectively: C-COOR (+0.4 eV); C—O (+1.6 eV); O-C=O (+3.9 eV), corresponding to chemical structure inset in Fig. 2D. In O1s spectra two oxygen moieties, C=O (~532.1 eV) and C-O-C (~533.5 eV) were found. The C1s and O1s core level spectra obtained for pPEA coatings (Fig. 2F and G) varied dramatically from SC-PEA, possessing lower concentrations of ester and carboxyl carbon binding environments, signified by loss of peaks in the spectra and definition of both corresponding oxygen peaks. From the carbon spectra (Fig. 2F), it can be noted that while the peak found at +1.6 eV from the backbone has almost entirely diminished the +3.9 eV peak is proportionally retained when plasma polymerised at lower energies. This relationship can be further observed in the oxygen spectra, which shows decreasing oxygen peaks correlating to the loss of these chemical sidechains. This translates to increased proportions of primary carbon binding relating to the PEA backbone, further enhancing and defining the 285 eV peak. However, the C1s spectra for all pPEA samples showed peaks at 285 eV (carbon-carbon backbone bond) and retention of small shoulder peaks at 288.9 eV (O-C=O bond), suggesting the pPEA coatings maintains some of the moieties characteristic of PEA (SC-PEA). This retention of functional groups is observed to relate to the power of polymerisation suggesting that increased energy directly influences the mechanism by which these peaks are lost, increasing the percentage of carbon backbone and decreasing the functional group composition on the top 10 nm of sample (Supp. Fig. 4). This chemical modification is characteristic of plasma discharge, resulting in monomer fragmentation, chain branching, cross linking and partial loss of functional groups during polymerisation [22,33,34]. More specifically, fragmentation, resulting from higher experimental powers producing a higher frequency and energy of electron impacts onto the polymerizing EA monomer, would provide an apt explanation for the resulting chemical variations of pPEA [35]. Therefore, we are able to conclude that plasma polymerisation produces oxygen deficient PEA coatings, with the level of remaining oxygen based functional groups directly depending on applied energy.

3.3. Maintenance of topographical roughness following pPEA nanocoating

Many biomedical applications, implants in particular, rely on creating and maintaining an interface with surrounding tissue. This tissue integration can be influenced and enhanced by surface roughness and patterned microstructures with many being developed specifically

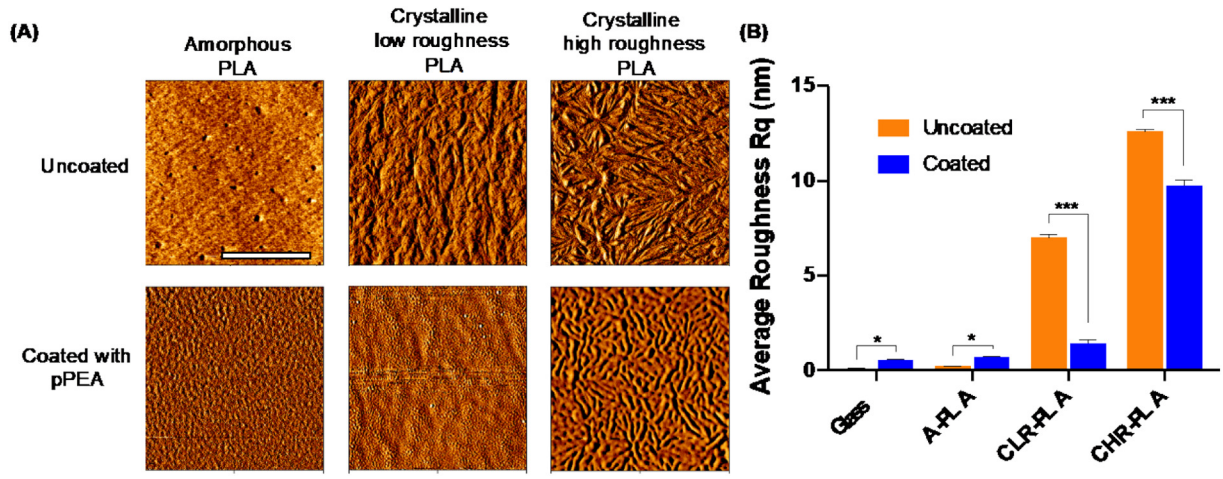

Fig. 3. (A) AFM phase scans of spin coated PLA surfaces with controlled roughness. Scale bar is 5 μm. (B) Measured average roughness Rq (nm) before and after coating with pPEA (180 kJ). Surfaces are glass, amorphous PLA (A-PLA), crystalline low roughness PLA (CLR-PLA), and crystalline high roughness PLA (CHR-PLA). CHR-PLA surfaces with higher roughness showed a decrease in roughness after coating but much smaller than on CLR-PLA, compared to substrate uncoated surfaces, demonstrating that a functional roughness can be maintained for CHR-PLA samples at these coating conditions.

for this goal [3]. We prepared spin coated amorphous and crystalline polylactic acid (PLA) surfaces with controlled surface roughness and then coated them with pPEA (180 kJ), measuring changes in average roughness after coating, to demonstrate conditions where the pPEA coatings could be applied while maintaining a functional roughness in the supporting material. AFM scans and roughness measurements (Fig. 3) show that the plasma deposition maintains surface roughness and features when the substrate's average roughness is as low as around 12 nm, including functional features that measure around 50 nm (Supp. Fig. 5). This preliminary study opens future developments to use pPEA coatings on functional surfaces without altering significantly the substrate roughness. For instance this would be the case for nanostructured surfaces used to manipulate stem cell differentiation, designed with pillars around 2 μm high and 200 nm in diameter [36] or functional roughness used on titanium implant surfaces to enhance bone integration [37]. Further control of substrate roughness, with smaller features preserved, could be achieved using shorter and lower power plasma depositions, as the experiments reported here were performed with our highest deposition energy and we have shown that much thinner coatings can be produced with lower energies.

3.4. Fibronectin and growth factor assembly on PEA coatings

Previous, work from our group has shown that PEA triggers spontaneous organisation of FN into nanonetworks which involves the simultaneous availability of the integrin binding region ($FNIII_{9–10}$) and growth factor (GF) binding region ($FNIII_{12–14}$) [28,29]. In this study, the interaction of pPEA coatings with FN was first studied to find out the capability of pPEA to maintain or promote FN fibrillogenesis as seen with bulk PEA (SC-PEA). Once pPEA and SC-PEA were coated onto glass coverslips and coated with FN (20 μg/mL), surface wettability was characterised by water contact angle, FN adsorption was characterised by AFM and micro BCA whilst FN domain availability and BMP-2 adsorption was characterised by ELISA. These experiments for protein adsorption and cell culture have used four selected plasma conditions (4.5, 15, 45 and 180 kJ). Fig. 4A shows the WCA measured on the PEA surfaces, with and without FN coatings. All pPEA and SC-PEA coatings are highly hydrophobic surfaces with water contact angle of around 73°–88°. However, all PEA surfaces show significantly different values to glass and became more hydrophilic once coated with FN. With FN coating the contact angle was observed within the range 40°–55°. On uncoated control glass surfaces, there is not much difference in wettability with or without FN coating. With respect to surface wettability of biologically active materials, cells effectively adhere onto surfaces presenting moderate wettability with water contact angles of 40°–70° [38,39]. However, the conformation and distribution of FN adsorption onto pPEA is very different to SC-PEA surfaces (Fig. 4B). AFM revealed these differences in the conformation of FN adsorbed on thin pPEA coatings compared with that on SC-PEA. Interconnected thin FN networks are organised upon adsorption from FN solution on SC-PEA whereas very dense compact FN network organised on all pPEA surfaces [29]. Presence of fibronectin on both SC-PEA and pPEA (45 kJ) was additionally confirmed using immunostaining (Supp. Fig. 6). SC-PEA samples showed dark spots absent of staining whereas pPEA images showed a continuous staining. This different organisation of FN is likely due to the differences in surface chemistry as well as the compositions of the polymers as shown by XPS analysis in particular.

Surface densities of the adsorbed FN on the different materials were further quantified using bicinchoninic acid assay (BCA). This was performed by measuring the amount of FN remaining in the supernatant after adsorption. Although the surface density of FN on all pPEA was slightly higher than that on SC-PEA and on glass surfaces, the difference was not significant (Fig. 4C). To evaluate the availability of integrin binding and GF binding domains on PEA surfaces after FN adsorption, an enzyme-linked immunosorbent assay (ELISA) using two monoclonal antibodies was used. HFN7.1 is directed against the flexible link between III_9 and III_{10} in $FNIII_{9–10}$ repeat of FN, which is involved in integrin binding and cell adhesion (Fig. 4D). P5F3 is directed against the $FNIII_{12–14}$ repeat which contributes to growth factor binding (Fig. 4E). Despite the surface density of FN on PEA and glass surfaces not being significantly different, we observed significantly higher availability of integrin and GF binding domains on pPEA in comparison to SC-PEA and glass surfaces (Fig. 4D and E). When these results were normalized to FN surface density, significant differences remained (Supp. Fig. 7), indicating that pPEA coatings increased levels of FN fibrillogenesis. These results suggest that FN assemble on pPEA surfaces into a dense network of nanofibrils that is functionally active to present simultaneously integrin binding and GF binding regions. We show that this property of pPEA is maintained regardless the condition used (energy in the plasma reactor) during plasma polymerisation.

In order to further elucidate how FN molecules organize on pPEA surfaces, we used lower concentrations (1 μg/mL and 500 ng/mL) in FN adsorption experiments. We hypothesised that a lower FN concentration would allow us better visualization of the conformation of FN on these surfaces. In Fig. 5 below, we see the conformation of FN on plasma polymerised materials at the aforementioned unusually low

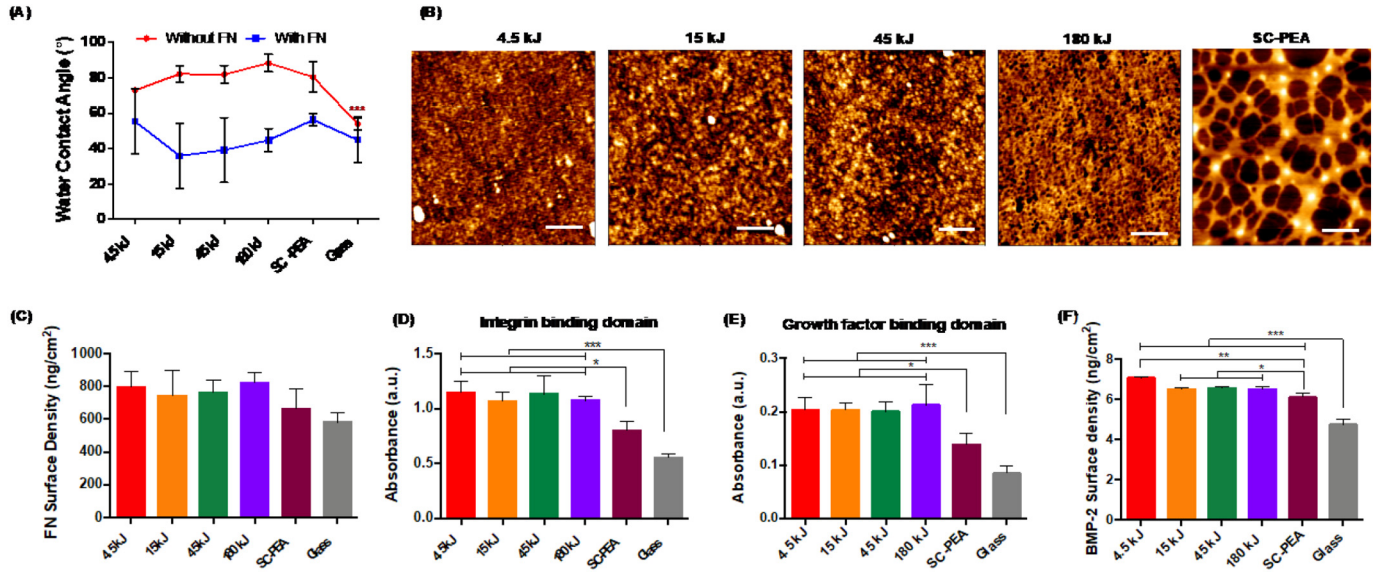

Fig. 4. Characterisation of PEA coatings before and after FN and BMP-2 adsorption. (A) Static water contact angle measurements of pPEA coatings, SC-PEA and glass surface with and without FN coating. Surfaces became more hydrophilic after absorption of FN. (B) AFM height images of pPEA and SC-PEA surfaces after FN coatings (20 μg/mL). Interconnected thin FN network was observed on SC-PEA, however thick dense FN networks were observed for all pPEA coatings. Scale bar is 200 nm. (C) Surface density of adsorbed FN on pPEA, SC-PEA and glass surface. All pPEA coatings showed higher FN adsorption compared to SC-PEA and glass surfaces. However, there is no significant difference between the samples. (D, E) Relative availability of integrin binding ($FNIII_{9-10}$) (D) and growth factor binding ($FNIII_{12-14}$) (E) domains on FN adsorbed on different surfaces, measured using ELISA. Both integrin and growth factor binding domain availability was significantly higher on pPEA coatings than on SC-PEA and glass surfaces. (F) Surface density of adsorbed BMP-2 on FN coated surfaces, measured by ELISA. All PEA coatings showing significant differences from SC-PEA and glass surfaces.

concentrations. Bundles of protein molecules seem to align or stretch over the surfaces in a distinctive manner different from the globular conformation of FN on other material surfaces.

We performed ELISA to assess whether the differential conformation of FN affects the surface density of BMP-2 bound on FN coated surfaces from a solution at a concentration of 50 ng/mL BMP-2. BMP-2 adsorption was significantly higher on pPEA surfaces than on SC-PEA and glass surfaces (Fig. 4F). This result supports the above data on GF binding domain availability, more BMP-2 adsorbed on FN coated on pPEA than on SC-PEA and glass surfaces.

3.5. Cell adhesion and differentiation

Human mesenchymal stem cells (MSCs) were cultured on PEA

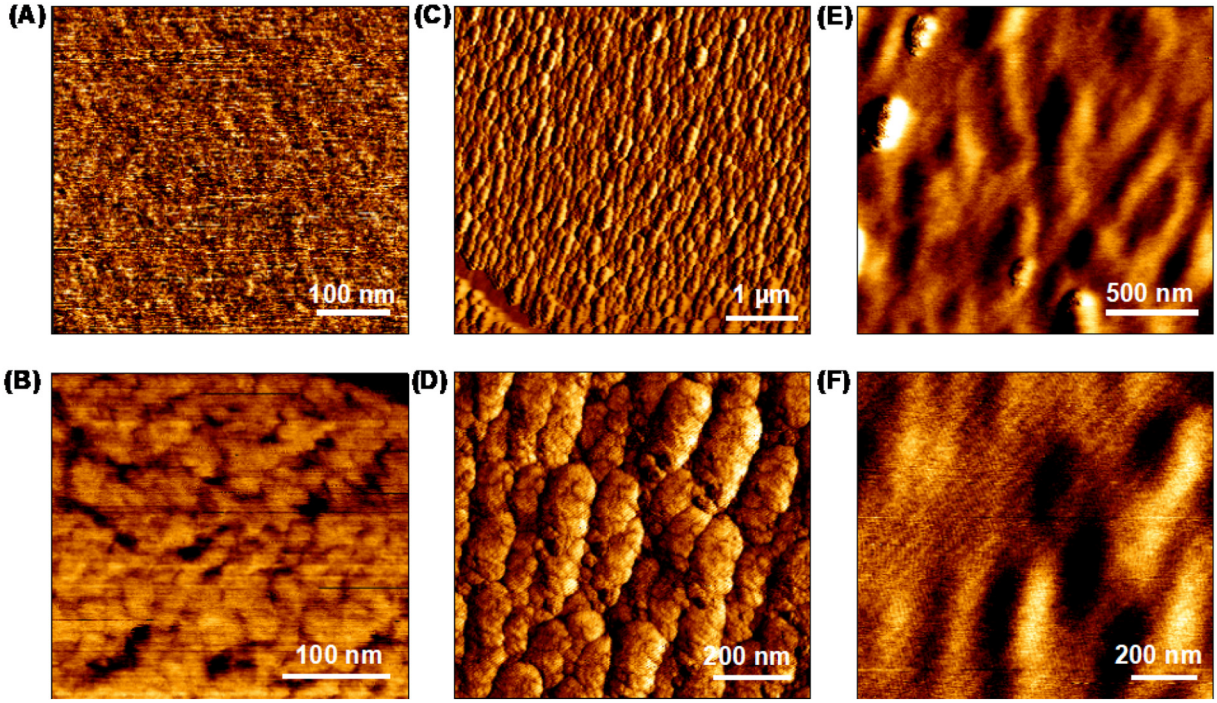

Fig. 5. AFM phase scans of adsorbed FN at low concentrations on pPEA (90 kJ) coated glass. (A) Reference surfaces shown are pPEA without adsorbed FN and (B) FN adsorbed at (20 μg/mL). (C) and (D) are surfaces with adsorbed FN at 1 μg/mL. (E) and (F) are surfaces with adsorbed FN at 500 ng/mL.

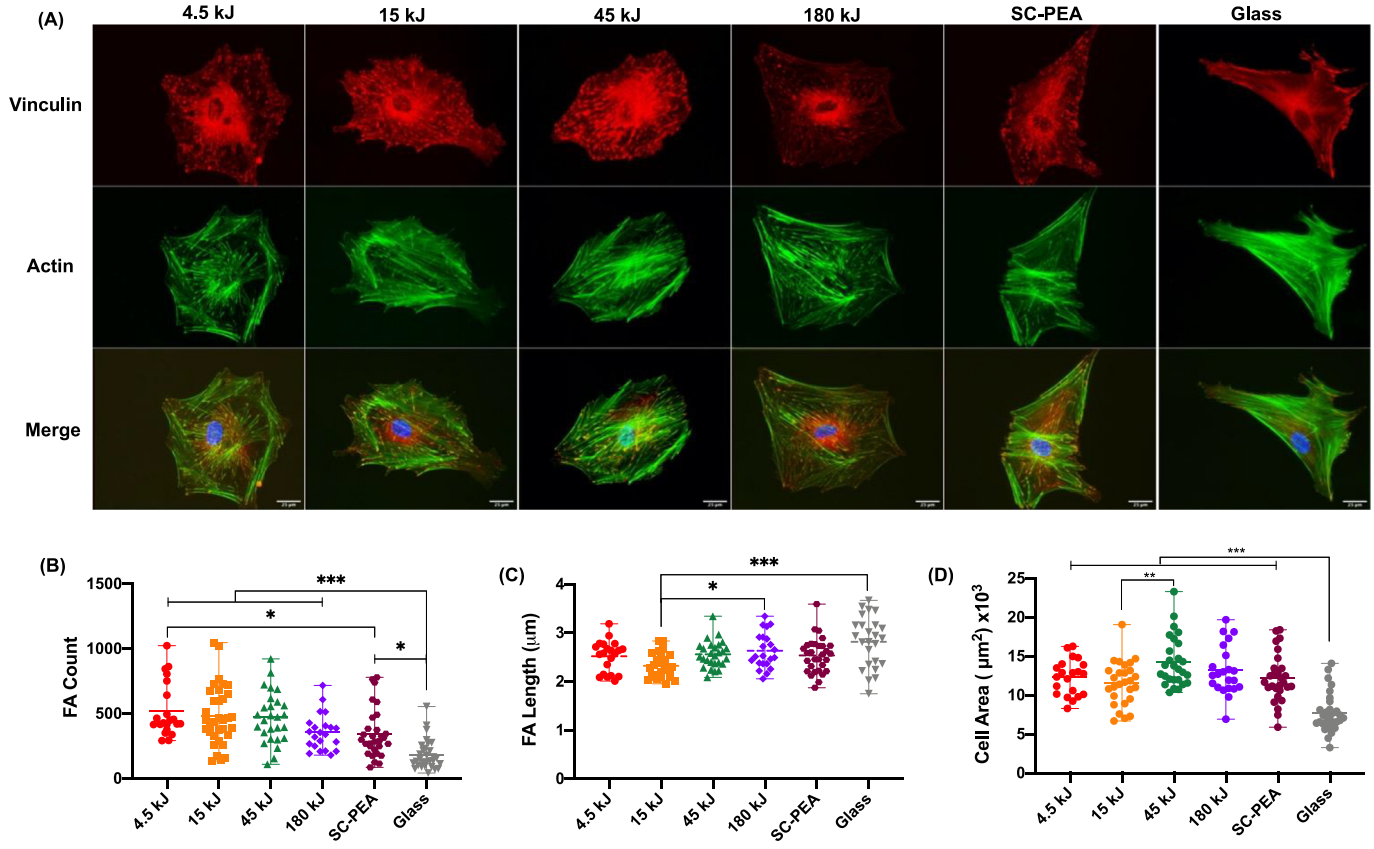

Fig. 6. Characterisation of hMSC focal adhesions on FN-coated PEA and glass surfaces. A) Immunostaining of vinculin (in red-top row), F-actin (in green-middle row) and merge image (bottom row). Scale bar is 25 μm. B) Total number of focal adhesion per cell on the different surfaces. Cells cultured on glass coverslips with FN coatings show significantly lower number of adhesions compared to cells on PEA with FN coated samples. (C) Focal adhesion average length (μm) on the different surfaces. (D) hMSC cell area in μm^2 for cells cultured in pPEA, spin-coated PEA and glass functionalized with FN. Cell area and FA count of cells cultured on PEA-FN surfaces show significantly higher values than on glass-FN surfaces. 20–30 cells per condition were analysed for each analysis. (For interpretation of the references to colour in this figure legend, the reader is referred to the web version of this article.)

surfaces coated with 20 μg/mL FN to evaluate initial cell response. Beside FN coated pPEA and SC-PEA, glass coverslips coated with FN were also used as controls. MSC adhesion was assessed through vinculin immunostaining, a protein present in focal adhesion complexes. Cell adhesion experiments were performed in the absence of serum in the culture media to make sure initial cell/material contact occurs only via interaction with adsorbed FN on the material substrates. Cells were seeded at a low density (5000 cells/cm^2) to minimize cell-cell and maximize cell-material interactions. Fig. 6A shows vinculin immunostaining on the FN coated surfaces after one day. Cells on all surfaces have spread and adhered and focal adhesions could be seen at the edges of the cell lamellae. The number of focal adhesions per cell was calculated from fluorescence microscopy images, using the data of at least 20–25 cells per condition. Fewer FA complexes were measured on glass surfaces (Fig. 6B) when compared to PEA surfaces. Average length of FA show similar for all surfaces which is 2.3–2.5 μm. Both cell area (Fig. 6D) and the number of FA for cells cultured on PEA-FN surfaces are significantly higher than in cells cultured on glass-FN surfaces. We hypothesize that this is due to the different conformation of the FN on the PEA surfaces, that allows for a higher exposure of the RGD domains in the unfolded fibronectin. It is noted that staining was carried out after 1 day as cells are expected to produce and rearrange ECM proteins at longer time points.

BMP-2 was next adsorbed on FN-coated PEA surfaces and MSC osteogenic differentiation quantified. Phenotypic characteristics of differentiated MSCs were assessed by real-time quantitative PCR of osteocalcin (OCN), osteopontin (OPN) and collagen type I (Col1A). Also von Kossa staining of calcium phosphate deposition, as part of matrix mineralisation, was assessed on PEA/FN/BMP-2 coated surfaces. Relative gene expression levels were measured by real time PCR after 28 days (Fig. 7A). Col1A and OPN are osteogenic markers associated with early osteogenic differentiation, whereas OCN is a late bone marker only secreted by osteoblasts cells. Cells cultured on FN coated surfaces (no BMP-2, 45 kJ and 180 kJ samples) show lower expression of osteogenic genes compared to BMP-2 coated surfaces (Supp. Fig. 8). It is worth noting that BMP-2 coated surfaces displayed significantly higher levels of the terminal osteoblast differentiation gene OCN [40] compared to FN only coated surfaces (Supp. Fig. 8C). All cells grown on BMP-2 coated surfaces showed detectable expression of the three aforementioned osteogenic markers OCN, OPN and Col1a, indicating their commitment towards a terminal osteogenic lineage.

Calcium phosphate deposits are a late marker of osteogenic differentiation and were assessed using von Kossa staining. Mineralisation was quantified for cells grown on different surfaces with and without BMP-2 coatings after 28 days. Cells cultured on FN coated surfaces (no BMP-2, 45 kJ and 180 kJ samples) show significantly lower levels of mineralisation compared to BMP-2 coated surfaces (Supp. Fig. 9). Samples with BMP-2 and PEA showed higher phosphate deposition than BMP-2 coated glass surface without PEA, as can be seen by the black deposits (Fig. 7Bi). Quantification of phosphate deposition shown in Fig. 7Bii again showed higher mineralisation in the PEA coated samples.

4. Conclusion

We show that PEA can be plasma polymerised into coatings (pPEA)

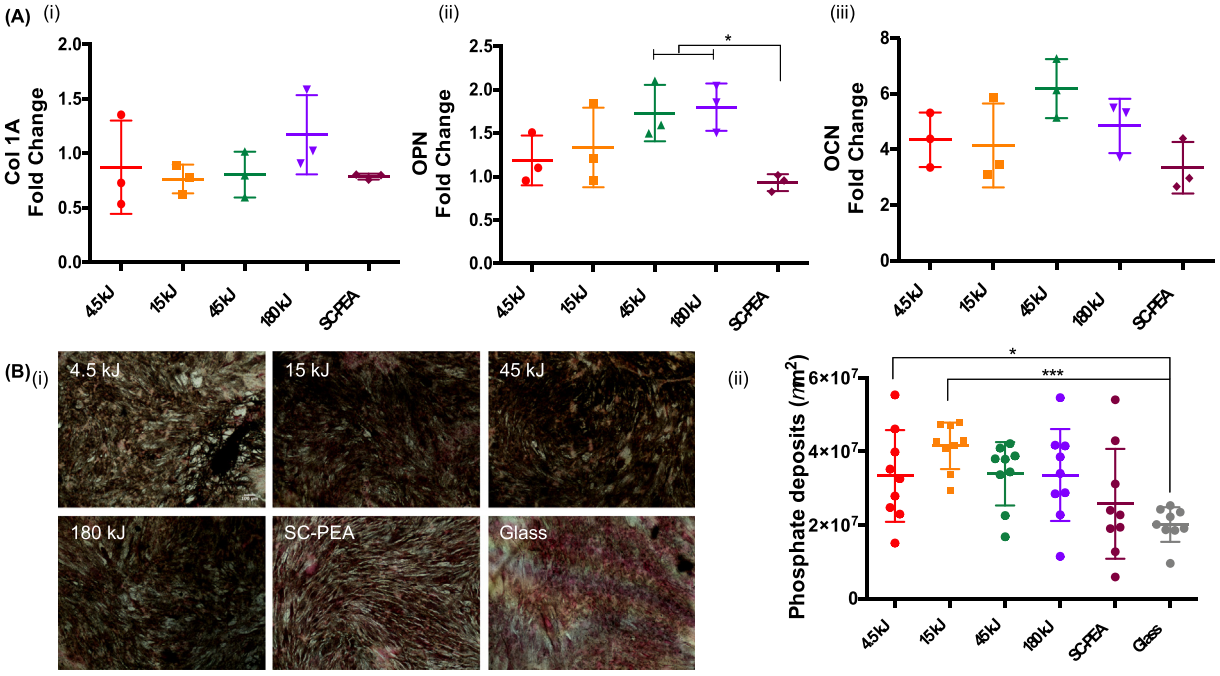

Fig. 7. Osteogenic differentiation of MSCs on PEA coated surfaces through gene expression and phosphate deposition. (A) q-PCR analysis for determination of the expression of osteogenic genes (i) Col1A, (ii) OPN, (iii) OCN with respect to control cultures (not PEA coated) on FN/BMP-2 coated surfaces after 28 days in culture. Controls only coated with PEA/FN can be found in the supplementary information. (B) Phosphate deposition (mineralisation) was assessed by von Kossa staining on surfaces coated with FN/BMP-2. Controls only coated with PEA/FN can be found in the supplementary information. Black nodules corresponding to phosphate deposition were imaged (i) and quantified by using image J software (ii) after 28 days in culture. Black area corresponding to phosphate deposits produced by the MSCs and red area corresponding to nuclear stain. All BMP-2 coated PEA surfaces show higher level of mineralisation compared to glass surfaces without PEA coating. A minimum of four images were taken from three technical replicates. Scale bar is 100 μm. (For interpretation of the references to colour in this figure legend, the reader is referred to the web version of this article.)

of controlled thickness that are bioactive. Thin coatings of between 30 and 300 nm were produced by changing the polymerisation energy provided by the plasma reactor. There is little influence of pPEA thickness on the ability to sequester BMP-2 and then induce MSC differentiation. Gene expression and mineralisation data demonstrates that the highest levels of differentiation are achieved when BMP-2 is adsorbed onto FN/PEA surfaces. Although modulation of FN assembly using PEA can alter cell morphology and osteogenesis, the addition of BMP-2 increases osteogenesis significantly. The thickness of the coating is such that the underlying topographical (roughness) features of the substrate are maintained. This work demonstrates the versatility of plasma polymerisation to provide polymer coatings of controlled thickness that can be used for solid phase presentation of growth factors. By nature, this process can be used to coat 2D and 3D surfaces with bioactive polymer [41]. The thickness control demonstrated here will also be important to modulate the degradation rate of the polymer film following in vivo implantation.

CRediT authorship contribution statement

Andres Alba:Conceptualization, Methodology, Data curation, Writing - original draft.**Vineetha Jayawarna**:Conceptualization, Methodology, Data curation, Writing - original draft.**Peter G. Childs**:Conceptualization, Methodology, Writing - review & editing.**Matthew J. Dalby**:Conceptualization, Supervision, Writing - review & editing.**Manuel Salmeron-Sanchez**:Conceptualization, Supervision, Funding acquisition, Writing - original draft.

Declaration of competing interest

The authors declare that they have no known competing financial interests or personal relationships that could have appeared to influence the work reported in this paper.

Acknowledgements

The support from the UK Engineering and Physical Sciences Research Council (EP/P001114/1) and the Sir Bobby Charlton Foundation is acknowledged. This work was also funded by a grant from the UK Regenerative Medicine Platform "Acellular / Smart Materials – 3D Architecture" (MR/R015651/1).

Appendix A. Supplementary data

Supplementary data to this article can be found online at https://doi.org/10.1016/j.msec.2020.110966.

References

[1] X. Hu, S.-H. Park, E.S. Gil, X.-X. Xia, A.S. Weiss, D.L. Kaplan, The influence of elasticity and surface roughness on myogenic and osteogenic-differentiation of cells on silk-elastin biomaterials, Biomaterials 32 (2011) 8979–8989, https://doi.org/10.1016/j.biomaterials.2011.08.037.
[2] F. Han, C. Zhu, Q. Guo, H. Yang, B. Li, Cellular modulation by the elasticity of biomaterials, J. Mater. Chem. B 4 (2016) 9–26, https://doi.org/10.1039/C5TB02077H.
[3] M.J. Dalby, N. Gadegaard, R.O.C. Oreffo, Harnessing nanotopography and integrin–matrix interactions to influence stem cell fate, Nat. Mater. 13 (2014) 558–569, https://doi.org/10.1038/nmat3980.
[4] S. Zangi, I. Hejazi, J. Seyfi, E. Hejazi, H.A. Khonakdar, S.M. Davachi, Tuning cell adhesion on polymeric and nanocomposite surfaces: role of topography versus superhydrophobicity, Mater. Sci. Eng. C. 63 (2016) 609–615, https://doi.org/10.1016/j.msec.2016.03.021.
[5] R. Fraioli, F. Rechenmacher, S. Neubauer, J.M. Manero, J. Gil, H. Kessler, C. Mas-Moruno, Mimicking bone extracellular matrix: integrin-binding peptidomimetics enhance osteoblast-like cells adhesion, proliferation, and differentiation on titanium, Colloids Surfaces B Biointerfaces 128 (2015) 191–200, https://doi.org/10.1016/j.colsurfb.2014.12.057.
[6] H. Gu, X. Chen, Q. Yu, X. Liu, W. Zhan, H. Chen, J.L. Brash, A multifunctional

surface for blood contact with fibrinolytic activity, ability to promote endothelial cell adhesion and inhibit smooth muscle cell adhesion, J. Mater. Chem. B 5 (2017) 604–611, https://doi.org/10.1039/C6TB02808J.
[7] Y.J. Chuah, Y.T. Koh, K. Lim, N.V. Menon, Y. Wu, Y. Kang, Simple surface engineering of polydimethylsiloxane with polydopamine for stabilized mesenchymal stem cell adhesion and multipotency, Sci. Rep. 5 (2016) 18162, , https://doi.org/10.1038/srep18162.
[8] Q. Huang, T.A. Elkhooly, X. Liu, R. Zhang, X. Yang, Z. Shen, Q. Feng, Effects of hierarchical micro/nano-topographies on the morphology, proliferation and differentiation of osteoblast-like cells, Colloids Surfaces B Biointerfaces 145 (2016) 37–45, https://doi.org/10.1016/j.colsurfb.2016.04.031.
[9] H. Elkhenany, L. Amelse, A. Lafont, S. Bourdo, M. Caldwell, N. Neilsen, E. Dervishi, O. Derek, A.S. Biris, D. Anderson, M. Dhar, Graphene supports in vitro proliferation and osteogenic differentiation of goat adult mesenchymal stem cells: potential for bone tissue engineering, J. Appl. Toxicol. 35 (2015) 367–374, https://doi.org/10.1002/jat.3024.
[10] A.A. John, A.P. Subramanian, M.V. Vellayappan, A. Balaji, S.K. Jaganathan, H. Mohandas, T. Paramalinggam, E. Supriyanto, M. Yusof, Review: physico-chemical modification as a versatile strategy for the biocompatibility enhancement of biomaterials, RSC Adv. 5 (2015) 39232–39244, https://doi.org/10.1039/C5RA03018H.
[11] E.D. de Avila, B.P. Lima, T. Sekiya, Y. Torii, T. Ogawa, W. Shi, R. Lux, Effect of UV-photofunctionalization on oral bacterial attachment and biofilm formation to titanium implant material, Biomaterials 67 (2015) 84–92, https://doi.org/10.1016/j.biomaterials.2015.07.030.
[12] K. Kasai, Y. Kimura, S. Miyata, Improvement of adhesion and proliferation of mouse embryonic stem cells cultured on ozone/UV surface-modified substrates, Mater. Sci. Eng. C. 78 (2017) 354–361, https://doi.org/10.1016/j.msec.2017.04.021.
[13] S.K. Jaganathan, A. Balaji, M.V. Vellayappan, A.P. Subramanian, A.A. John, M.K. Asokan, E. Supriyanto, Review: radiation-induced surface modification of polymers for biomaterial application, J. Mater. Sci. 50 (2015) 2007–2018, https://doi.org/10.1007/s10853-014-8718-x.
[14] T. Zhou, Y. Zhu, X. Li, X. Liu, K.W.K. Yeung, S. Wu, X. Wang, Z. Cui, X. Yang, P.K. Chu, Surface functionalization of biomaterials by radical polymerization, Prog. Mater. Sci. 83 (2016) 191–235, https://doi.org/10.1016/j.pmatsci.2016.04.005.
[15] G. Aziz, R. Ghobeira, R. Morent, N. De Geyter, Plasma polymerization for tissue engineering purposes, Recent Res. Polym, InTech, 2018, , https://doi.org/10.5772/intechopen.72293.
[16] H. Thissen, Plasma-based surface modification for the control of biointerfacial interactions, Biosynthetic Polym. Med. Appl, Elsevier, 2016, pp. 129–144, , https://doi.org/10.1016/B978-1-78242-105-4.00005-5.
[17] M.R. Sprott, G. Gallego-Ferrer, M.J. Dalby, M. Salmerón-Sánchez, M. Cantini, Functionalization of PLLA with polymer brushes to trigger the assembly of fibronectin into nanonetworks, Adv. Healthc. Mater. (2019) 1801469, , https://doi.org/10.1002/adhm.201801469.
[18] P. Chu, Plasma-surface modification of biomaterials, Mater. Sci. Eng. R Reports. 36 (2002) 143–206, https://doi.org/10.1016/S0927-796X(02)00004-9.
[19] M. Macgregor, K. Vasilev, Perspective on plasma polymers for applied biomaterials nanoengineering and the recent rise of oxazolines, Materials (Basel) 12 (2019) 191, https://doi.org/10.3390/ma12010191.
[20] S. Bhatt, J. Pulpytel, F. Arefi-Khonsari, Low and atmospheric plasma polymerisation of nanocoatings for bio-applications, Surf. Innov. 3 (2015) 63–83, https://doi.org/10.1680/sufi.14.00008.
[21] H. Yasuda, T.S. Hsu, Some aspects of plasma polymerization of fluorine-containing organic compounds, J. Polym. Sci. Polym. Chem. Ed. 15 (1977) 2411–2425, https://doi.org/10.1002/pol.1977.170151011.
[22] H. Yasuda, M. Gazicki, Biomedical applications of plasma polymerization and plasma treatment of polymer surfaces, Biomaterials 3 (1982) 68–77, https://doi.org/10.1016/0142-9612(82)90036-9.
[23] S. Babaei, N. Fekete, C.A. Hoesli, P.-L. Girard-Lauriault, Adhesion of human monocytes to oxygen- and nitrogen- containing plasma polymers: effect of surface chemistry and protein adsorption, Colloids Surfaces B Biointerfaces 162 (2018) 362–369, https://doi.org/10.1016/j.colsurfb.2017.12.003.
[24] M. Zelzer, R. Majani, J.W. Bradley, F.R.A.J. Rose, M.C. Davies, M.R. Alexander, Investigation of cell–surface interactions using chemical gradients formed from plasma polymers, Biomaterials 29 (2008) 172–184, https://doi.org/10.1016/j.biomaterials.2007.09.026.
[25] Jin Ho Lee, Jong Woo Park, Hai Bang Lee, Cell adhesion and growth on polymer surfaces with hydroxyl groups prepared by water vapour plasma treatment, Biomaterials 12 (1991) 443–448, https://doi.org/10.1016/0142-9612(91)90140-6.
[26] R.M. France, R.D. Short, R.A. Dawson, S. Macneil, Attachment of human keratinocytes to plasma co-polymers of acrylic acid/octa-1,7-diene and allyl amine/octa-1,7-diene, J. Mater. Chem. 8 (1998) 37–42, https://doi.org/10.1039/a705098d.
[27] P. Rossini, P. Colpo, G. Ceccone, K. Jandt, F. Rossi, Surfaces engineering of polymeric films for biomedical applications, Mater. Sci. Eng. C. 23 (2003) 353–358, https://doi.org/10.1016/S0928-4931(02)00286-2.
[28] V. Llopis-Hernández, M. Cantini, C. González-García, Z.A. Cheng, J. Yang, P.M. Tsimbouri, A.J. García, M.J. Dalby, M. Salmerón-Sánchez, Material-driven fibronectin assembly for high-efficiency presentation of growth factors, Sci. Adv. 2 (2016) e1600188, , https://doi.org/10.1126/sciadv.1600188.
[29] Z.A. Cheng, A. Alba-Perez, C. Gonzalez-Garcia, H. Donnelly, V. Llopis-Hernandez, V. Jayawarna, P. Childs, D.W. Shields, M. Cantini, L. Ruiz-Cantu, A. Reid, J.F.C. Windmill, E.S. Addison, S. Corr, W.G. Marshall, M.J. Dalby, M. Salmeron-Sanchez, Nanoscale coatings for ultralow dose BMP-2-driven regeneration of critical-sized bone defects, Adv. Sci. 6 (2019) 1800361, , https://doi.org/10.1002/advs.201800361.
[30] Y.V.P.C.M.K.K.L.-S.S.S.D.D.D. Ratner, Micro-scale cell patterning on nonfouling plasma polymerized tetraglyme coatings by protein microcontact printing, Plasmas Polym. 7 (2002) 171–183, https://doi.org/10.1023/A:1016295419941.
[31] K.S. Siow, L. Britcher, S. Kumar, H.J. Griesser, Plasma methods for the generation of chemically reactive surfaces for biomolecule immobilization and cell colonization - a review, Plasma Process. Polym. 3 (2006) 392–418, https://doi.org/10.1002/ppap.200600021.
[32] J.F. Watts, G. Beamson, D. Briggs (Eds.), High Resolution XPS of Organic Polymers: The Scienta ESCA 300 Database, John Wiley & Sons, Chichester, 1992, p. 267.
[33] M. Cantini, P. Rico, D. Moratal, M. Salmerón-Sánchez, Controlled wettability, same chemistry: biological activity of plasma-polymerized coatings, Soft Matter 8 (2012) 5575, https://doi.org/10.1039/c2sm25413a.
[34] E.J. Szili, R.D. Short, D.A. Steele, J.W. Bradley, Surface modification of biomaterials by plasma polymerization, Surf. Modif. Biomater, Elsevier, 2011, pp. 3–39, , https://doi.org/10.1533/9780857090768.1.3.
[35] A. Michelmore, P. Gross-Kosche, S.A. Al-Bataineh, J.D. Whittle, R.D. Short, On the effect of monomer chemistry on growth mechanisms of nonfouling PEG-like plasma polymers, Langmuir 29 (2013) 2595–2601, https://doi.org/10.1021/la304713b.
[36] R.J. McMurray, N. Gadegaard, P.M. Tsimbouri, K.V. Burgess, L.E. McNamara, R. Tare, K. Murawski, E. Kingham, R.O.C. Oreffo, M.J. Dalby, Nanoscale surfaces for the long-term maintenance of mesenchymal stem cell phenotype and multipotency, Nat. Mater. 10 (2011) 637–644, https://doi.org/10.1038/nmat3058.
[37] T.A.A. Wennerberg, On implant surfaces: a review of current knowledge and opinions, Int J Oral Maxillofac Implant 25 (2010) 63–74.
[38] Y. Arima, H. Iwata, Effect of wettability and surface functional groups on protein adsorption and cell adhesion using well-defined mixed self-assembled monolayers, Biomaterials 28 (2007) 3074–3082, https://doi.org/10.1016/j.biomaterials.2007.03.013.
[39] C. Kleinhans, J. Barz, S. Wurster, M. Willig, C. Oehr, M. Müller, H. Walles, T. Hirth, P.J. Kluger, Ammonia plasma treatment of polystyrene surfaces enhances proliferation of primary human mesenchymal stem cells and human endothelial cells, Biotechnol. J. 8 (2013) 327–337, https://doi.org/10.1002/biot.201200210.
[40] R.P. Tracy, A. Andrianorivo, B.L. Riggs, K.G. Mann, Comparison of monoclonal and polyclonal antibody-based immunoassays for osteocalcin: a study of sources of variation in assay results, J. Bone Miner. Res. 5 (1990) 451–461, https://doi.org/10.1002/jbmr.5650050506.
[41] C. Canal, K. Khurana, S. Gallinetti, S. Bhatt, J. Pulpytel, F. Arefi-Khonsari, M.P. Ginebra, Design of calcium phosphate scaffolds with controlled simvastatin release by plasma polymerisation, Polymer (Guildf). 92 (2016) 170–178, https://doi.org/10.1016/j.polymer.2016.03.069.